



Developments in the Built Environment

journal homepage: www.sciencedirect.com/journal/developments-in-the-built-environment

Damage evolution and avalanche characteristics of concrete under salt-freezing action by acoustic emission

Yunfeng Zhao ^a, Minghui Chen ^{a,*}, Xiang Jiang ^b, Xuepeng Cao ^a, Binbin Qin ^c^a School of Urban Construction, Yangtze University, Jingzhou, 434000, China^b School of Materials Science and Engineering, Chongqing Jiaotong University, Chongqing, 400074, China^c School of Economics and Management, Yangtze University, Jingzhou, 434023, China

ARTICLE INFO

ABSTRACT

Keywords:

Salt-freezing action
Concrete
Acoustic emission
Avalanche characteristics
B-value

Concrete structures in saline-alkali areas will suffer from salt freezing and cause diseases. In this paper, experiments of concrete deterioration under the coupling action of sulfate attack and freeze-thaw cycles were carried out. The avalanche characteristics of acoustic emission (AE) signals generated during concrete failure were analyzed statistically by avalanche dynamics theory, and compared with traditional AE analysis methods. The results show that with the increase of cycle times, the proportion of shear cracks in the failure process of concrete specimens gradually increases, and the AE *b*-value increases. The energy distribution exponent, amplitude distribution exponent, and duration distribution exponent of concrete specimens gradually increase, while the correlation exponent between amplitude and absolute energy decreases, and the correlation exponent between duration and amplitude fluctuates within a certain range. The distribution exponent of waiting time shows robustness. Avalanche exponents can be applied to the quantitative characterization of concrete damage under the salt-freezing action.

1. Introduction

The Food and Agriculture Organization of the United Nations estimates that there are more than 833 million hectares (8.7% of the Earth's surface area) of saline land worldwide, mostly in arid or semi-arid regions of Africa, Asia, and Latin America ([Home Global Symposium on Salt-affected Soils; Gong et al., 2023](#)). Among them, the soil in the dry and cold areas of northwest China is rich in corrosive sulfate ions, and the climate is characterized by low temperatures and large temperature differences between day and night. In water conservancy projects in such areas, concrete structures are often subjected to sulfate erosion and freeze-thaw cycles during service. The chemical attack of sulfate solution ([Müllauer et al., 2013; Bizzozero et al., 2014](#)) and the physical attack of freeze-thaw cycle ([Luo et al., 2018; Sun et al., 2019](#)) can lead to the disease and even failure of concrete structure. The deterioration of concrete under the coupled action of sulfate attack and the freeze-thaw cycles is not a simple superposition of the two, and the mutual promotion between the two will accelerate the damage and destruction of concrete ([Jiang et al., 2015](#)). It is of great significance to study the damage and deterioration of concrete under the coupling action of sulfate attack and freeze-thaw cycles for the durability design and disease

prevention of concrete structures in these areas.

At present, many scholars have studied the durability and damage characteristics of concrete under the action of salt freezing, as well as exploring new environmentally friendly high-performance concrete ([Qaidi et al., 2021, 2022](#)). Among them, the research on concrete durability mainly focuses on the salt-freeze resistance of modified concrete, such as concrete containing additives ([Wang et al., 2017; Zhao et al., 2020](#)), cement mortar ([Adediran et al., 2022](#)), basalt fiber geopolymer concrete ([Bian et al., 2024](#)), high-performance ecological geopolymer concrete ([Bao et al., 2024](#)), PVA fiber reinforced geopolymer concrete ([Zhao et al., 2021a](#)), and recycled concrete ([Zheng et al., 2024](#)). On the other hand, the damage characteristics of concrete under the action of salt freezing are mainly developed from the aspects of macroscopic physical and mechanical properties, mesoscopic pore structure evolution, and damage model ([Xiao et al., 2019; Xue et al., 2024; Chen et al., 2021; Hu and Yin, 2022; Wei et al., 2024; Gan et al., 2023](#)). The research on the fracture performance of concrete under the action of salt freezing points out ([Hu and Yin, 2022](#)) that with the increase of the number of freeze-thaw cycles, the obtained double-K fracture parameters, the length of the micro-crack zone, and the aggregate block zone all linearly decrease. The compressive strength,

* Corresponding author.

E-mail address: chenminghui.stu@yangtzeu.edu.cn (M. Chen).

splitting tensile strength, and relative dynamic modulus of concrete under the action of alternating salt and freeze show a decreasing trend, and the mechanical properties of concrete gradually decrease with the increase of sulfate solution concentration. With the increase of the number of alternating salt-freeze cycles, the fractal dimension of concrete pores gradually decreases and the porosity gradually increases (Gan et al., 2023).

The study of the macroscopic damage characteristics of concrete under the action of salt-freezing provides support for its durability design, while the microscopic damage can better reflect the damage evolution process and failure mechanism. Acoustic emission (AE) technology is used to monitor the signals generated during the concrete failure process, which provides a means to study the damage evolution of concrete at the meso-level. Attention has been paid to AE analysis of concrete damage under different environmental factors, such as freeze-thaw, salt corrosion, etc., mainly focusing on AE count, energy, amplitude, frequency, and other parameters as well as RA-AF (RA = rise time/amplitude, AF = acoustic emission count/duration) and *b*-value statistics (Choi and Yun, 2015; Xu et al., 2023; Liu et al., 2023, 2024; He et al., 2023; Qiao et al., 2015; Li et al., 2022; Lian et al., 2023; Bai et al., 2023a, 2023b; Zhang et al., 2024). Choi et al. (Choi and Yun, 2015) pointed out that AE activities such as ringing count, energy, amplitude, frequency, and other parameters can characterize the mesoscopic damage of carbon fiber-reinforced concrete beams. Xu et al. (2023) studied the fracture behavior of concrete under freeze-thaw action, and the results showed that the changes of AE cumulative count, energy and *b*-value correspond to the three divided concrete failure stages, and AE count can be used to establish a damage model to characterize freeze-thaw damage. Liu et al. (2024) studied the AE characteristics of concrete under sulfate attack, and the results showed that the stronger the AE activity under high concentration sulfate attack, the *b*-value would decrease in the later stage of concrete failure. At present, there are few studies on AE characteristics of concrete under the coupling of multiple environmental factors, such as the salt-freezing action, and the above traditional AE analysis is mainly qualitative evaluation, and there is no fixed theoretical value of *b*-value.

In recent years, avalanche dynamics analysis of complex physical systems derived from natural avalanche phenomena has been introduced into the research field of material damage and failure. The avalanche effect is defined as the process in which the interaction between a series of small events is amplified across scales to cause sudden large events when the system is in a self-organized critical state (Sethna et al., 2001; Salje and Dahmen, 2014). The material failure process is essentially a series of interactions between small displacements or force drops, which results in large displacements leading to failure and instability through cross-scale amplification, which accords with the characteristics of the avalanche effect. The large and small avalanche events are not isolated but meet certain distribution rules. Statistical analysis of the avalanche characteristics of AE signals generated during the failure of coal (Jiang et al., 2016; Xu et al., 2019), sandstone (Zhao et al., 2019; Jiang et al., 2019; Salje et al., 2018), granite (Xie et al., 2019), alloy (Chen et al., 2019, 2022), teeth (Wang et al., 2021), etc., shows that the probability density distribution of AE parameters conforms to the power law, and the corresponding power law exponent, that is, the avalanche exponent, is different, which is related to the internal microstructure and failure mechanism of the material. For the deterioration and failure process of concrete under environment and load, it contains the fracture of cement matrix and aggregate, as well as interfacial debonding and dislocation. At the micro level, it is pore collapse, resulting in micro-cracks. On the macro level, it turns into deformation or displacement, and can be described by softening behavior or catastrophic snap-back in the load-displacement curve. It is a series of chain reactions from the initial micro-crack to the final concrete failure. This physical trigger mechanism conforms to the avalanche effect, and the released cross scale energy signal also conforms to the extended avalanche concept. Previous studies (Zhao et al., 2021b, 2022) on the

avalanche characteristics of concrete under sulfate attack show that the statistical characteristics are also power law, where the energy distribution exponent is related to the degree of sulfate attack.

In general, the study of avalanche characteristics of concrete degradation failure process at the microscale based on AE can better reflect the damage evolution process and failure mechanism. At present, only the avalanche characteristics of concrete under single sulfate erosion have been studied, and the multi-factor coupling effect is rarely studied. Therefore, the damage and deterioration of concrete under the salt-freezing action are studied in this paper, and the avalanche characteristics of AE signals are analyzed statistically, and compared with the traditional *b*-value statistics. It provides a reference for the prevention and control of concrete structure disease in saline-alkali area, and further enriches the AE analysis method in the study of material damage.

2. Materials and methods

2.1. Specimen preparation

P.O.42.5 ordinary Portland cement was used as the main cementing material for concrete specimens, and its composition is shown in Table 1. The fine aggregate is natural river sand (fineness modulus is 2.7), and the coarse aggregate is limestone gravel (particle size 5~22.5 mm) from the Jining mine in Shandong Province. According to the "Ordinary Concrete Mix Design Code" (JGJ55-2019), the mixture proportions of concrete specimens are shown in Table 2. The mixture proportion comes from the construction site. Compared with the standard mixture proportion, the increase in the proportion of mineral powder and fly ash has improved the durability and resistance to sulfate attack of concrete, thus meeting the requirements of the test conditions. Molds with sizes of 100 mm × 100 mm × 400 mm and 100 mm × 100 mm × 100 mm were used to prepare the concrete specimens. The molds were removed 24 h later and the concrete specimens were placed in a standard curing box for 28 d. Among them, the temperature and relative humidity were controlled at 20 °C ± 2 °C and ≥95%, respectively. The cured concrete specimens were cored, cut, and polished to produce a cylindrical specimen with a size of 50 mm × 100 mm. Ensure that the parallelism deviation of the end face of the specimen was not more than 0.1 mm and the diameter deviation was not more than 0.2 mm, as shown in Fig. 1.

2.2. Freeze–thaw cycles in water and sulfate solution

According to the "Experimental Method for Long-term Performance and Durability of Ordinary Concrete" (GB J82-85), the freeze-thaw cycle test of concrete was carried out by using the rapid freeze-thaw method. The sulfate concentration in most real environments is low, and the deterioration process of concrete under sulfate attack takes a long time, up to several years or decades. In order to shorten the laboratory test period, the erosion process was accelerated by increasing the sulfate concentration. Na₂SO₄ solution with a mass fraction of 5% was used as freeze-thaw solution, and a clean water group was set for control. Before the freeze-thaw cycle test, the concrete specimens of the Na₂SO₄ solution group and clean water group were soaked in the corresponding solution respectively for 4 days under the constant temperature condition of 20 °C. The number of freeze-thaw cycles set in this test was 0, 25, 50, 75, 100, and 200 times respectively, and the TDRF-2 rapid freeze-thaw testing machine was used. This machine simulates the freeze-thaw cycle by injecting antifreeze into the specimen box and using a refrigerator and heater to cool and heat the antifreeze. Temperature sensors are placed at the center of the antifreeze in the freeze-thaw chamber, at both ends of the center and any diagonal line, to collect temperature information of the antifreeze. Each freeze-thaw cycle was completed in 4 h, and the melting time was not less than 1/4 of the entire freeze-thaw cycle time. During the freeze-thaw process, the upper limit and lower limit of the center temperature of the specimen were

Table 1

Chemical composition of the ordinary Portland cement.

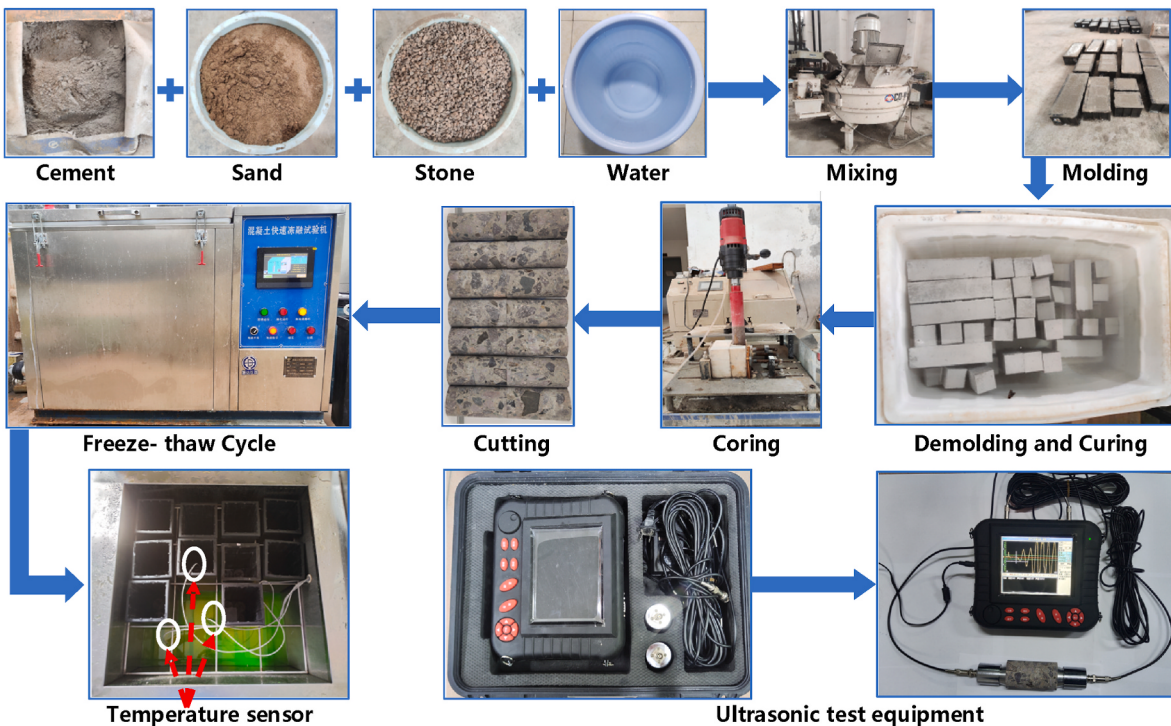
Composition	SiO ₂	Al ₂ O ₃	Fe ₂ O ₃	MgO	CaO	Na ₂ O	K ₂ O	SO ₃	LOI
Mass ratio(%)	20.4	51.4	4.4	1.31	62.8	0.42	0.28	2.48	2.39

Note: LOI = loss in ignition.

Table 2

Mixture proportions per cubic meter.

Materials	Cement	Water	Fly ash	Fine aggregate	Coarse aggregate	Mineral powder	Water reducer
Content (kg/m ³)	423	167	43	689	952	76	13.6

**Fig. 1.** Preparation of specimens, freeze-thaw cycle, and UPV test.

controlled at $(5 \pm 2)^\circ\text{C}$ and $(-18 \pm 2)^\circ\text{C}$, respectively, and the Na₂SO₄ solution was replaced regularly to maintain a stable pH value and sulfate ion concentration.

2.3. Physical mechanical properties and AE monitoring

When the concrete specimens reached the set number of cycles, took it out and dried the surface water and let it dry naturally for 1 d, and then measured the mass and ultrasonic pulse velocity (UPV) of the specimens. The mass loss rate of concrete specimens is:

$$S_m = (M_0 - M_n) / M_0 \times 100\% \quad (1)$$

Where S_m is the mass loss rate, M_0 is the initial mass, and M_n is the mass after the Nth freeze-thaw cycle.

The uniaxial compression test was carried out on concrete specimens that reached the set number of freeze-thaw cycles, and the test equipment was the HYAS-1000C rock triaxial test system. The displacement loading method was adopted in the test, and the loading rate was 0.003 mm/s. Four RS-2A ceramic surface AE sensors produced by Softland Times were symmetrically arranged on the surface of concrete specimens, with a diameter of 18.8 mm. To ensure the reliability of signal transmission between the sensor and the cylindrical specimen, the

sensor was placed in a specially designed component similar to a waveguide rod, with a contact surface diameter of 8 mm between the specially designed component and the sample. The contact surfaces between the sensor and the specially designed component, as well as between the specially designed component and the sample, were coated with a coupling agent (Vaseline). The AE test system DS5 was used to collect AE signals generated during the uniaxial compression test, as shown in Fig. 2. The ambient noise measured by the AE sensor was about 40 dB, and the threshold was set to 45 dB to filter the background noise. The main parameters of the AE test system are shown in Table 3. The schematic diagram of AE monitoring is shown in Fig. 3.

2.4. X-ray diffraction and SEM

The composition and microstructure of concrete specimens with 0, 50, 75, 100, and 200 freeze-thaw cycles in Na₂SO₄ solution were detected by X-ray diffraction (XRD) and SEM. The SEM was equipped with the EDS for Energy Dispersive X-ray spectrometry. For the SEM observation in this study, powder specimens of representative concrete were examined in low vacuum mode with an acceleration voltage of 15 keV and the corresponding working distance of 0 cycle, 75 cycles, and 200 cycles was 7.45 mm, 7.86 mm, and 8.15 mm respectively. A

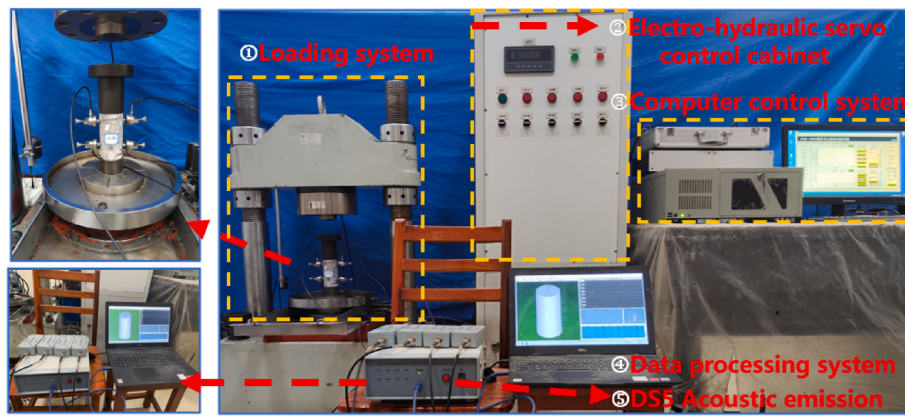


Fig. 2. Uniaxial compression test and AE monitoring.

Table 3
Parameters of AE test system.

Test parameter	Set value
Sensor resonant frequency	150–400 kHz
Threshold for detection	45 dB
PDT	35μs
HDT	150μs
HLT	300μs
Sampling frequency	3 MHz
Pre-gain	40 dB

counting rate of about 3500 counts per second and a step size of 0.02 were used for EDX analysis. For EDS operation, it is necessary to take an appropriate amount of specimen and place it in the center of the specimen table and apply it with a glass sheet so that it fills the specimen table groove.

3. Results

3.1. Composition and microstructure

XRD is used to analyze the composition of concrete specimens after salt-freezing action, and the XRD patterns under different cycles are shown in Fig. 4. The XRD patterns of the specimens in the initial 50 cycles are mainly diffraction peaks of dicalcium silicate (Ca_2SiO_4) and calcium sulfate (CaSO_4), and the intensity of the diffraction peaks of dicalcium silicate (Ca_2SiO_4) is higher, and the composition of the specimens has no obvious change. The diffraction peak of calcium sulfate (CaSO_4) in the specimen was pretreated by soaking Na_2SO_4 solution before the test. After 75 cycles, the diffraction peak intensity of calcium sulfate (CaSO_4) increased to 4809. After 200 cycles, the XRD pattern of the specimen is mainly the diffraction peak of calcium sulfate (CaSO_4),

and the diffraction peak intensity increased significantly to 7295.

Microstructure analysis is carried out on concrete specimens after salt-freezing action under different cycles, as shown in Fig. 5. There are pores and cracks in the concrete specimen before the freeze-thaw cycle, which is a typical porous material. After 75 cycles, the surface morphology of the specimen shows the adhesion of sulfate corrosion products. After 200 cycles, there was enrichment of sulfate corrosion products, and internal cracks expand and pores increase. The effect of salt-freezing action on the internal microstructure of concrete is significant.

3.2. Physical mechanical properties

Fig. 6 shows the relationship between compressive strength, mass loss rate, and UPV of concrete specimens in Na_2SO_4 solution and clean water with the number of freeze-thaw cycles. Under the condition of Na_2SO_4 solution and clean water, the compressive strength and UPV of concrete specimens decrease with the increase of the number of cycles, and the mass loss rate increases. After 50 cycles, the compressive strength and UPV of the concrete specimens in the Na_2SO_4 solution group are reduced by 6.2% and 5.0% respectively, while the concrete specimens in the clean water group are reduced by 11.1% and 10.0% respectively. After 200 cycles, the compressive strength and UPV of the concrete specimens in the Na_2SO_4 solution group are reduced by 50.6% and 62.2% respectively, while the concrete specimens in the clean water group are reduced by 38.3% and 41.8% respectively. The mass loss rates of concrete specimens of the Na_2SO_4 solution group and clean water group corresponding to 50 and 200 cycles are 1.0% and 5.1%, respectively, and 1.4% and 3.9%, respectively. The result shows that in the initial 50 cycles, the compressive strength, UPV, and mass of the concrete specimens in the clean water group decreased more, while in the Na_2SO_4 solution group decreased faster after 75 cycles. At the early stage of the freeze-thaw cycle, the damage degree of the concrete specimens in

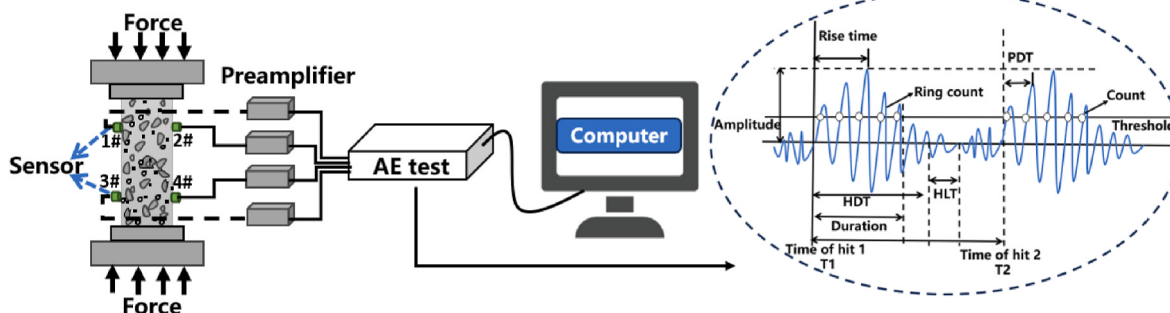


Fig. 3. Schematic diagram of AE monitoring.

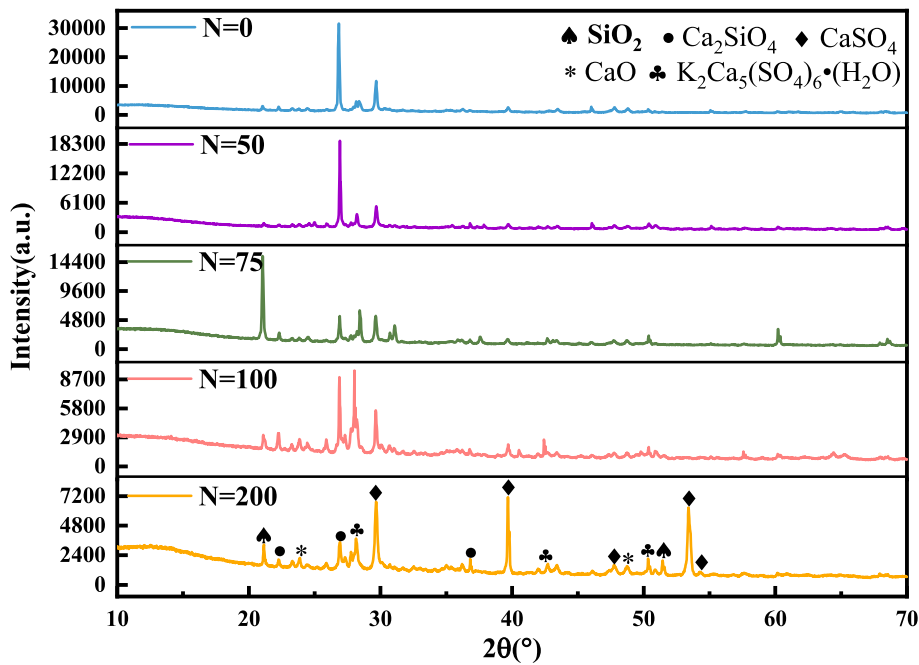


Fig. 4. XRD pattern of concrete specimens with different cycles under salt-freezing action.

the clean water group is greater, which indicates that the early sulfate erosion in the Na_2SO_4 solution group has a certain inhibition effect on the freeze-thaw damage. In the test, the freezing point of Na_2SO_4 solution is lower than the clean water, and its crystallization pressure (frost heave force and salt heave force) is lower than the clean water, and the chemical reaction in the early stage of sulfate attack is not significant (as shown in Fig. 5). After 75 cycles, the damage degree of concrete specimens in the Na_2SO_4 solution group is larger and increases rapidly, indicating that the damage in the Na_2SO_4 solution group is mutually promoted by sulfate erosion and freeze-thaw cycle. Under the action of frost heave force, the internal pores of concrete specimens increase and cracks penetrate, and sulfate ions are more likely to enter the interior of concrete, causing chemical erosion. A large amount of gypsum, the product of expansion erosion, accumulates in the pores (as shown in Fig. 5), resulting in increased pore stress, further promoting the generation of cracks, and rapidly increasing the damage degree of concrete specimens.

3.3. Stress-time relationship and AE energy spectrum

The stress-time relationship and AE energy spectrum of concrete specimens of the Na_2SO_4 solution group and clean water group under different freeze-thaw cycles are shown in Fig. 7. Considering the influence of the number of AE signals on the subsequent statistical analysis, the AE data of the sensor receiving the most signals was selected for statistical analysis. The peak stress of the two groups of concrete specimens decreases with the increase of the number of freeze-thaw cycles. Under different freeze-thaw cycles, the AE signals of the two groups of concrete specimens are the densest near the peak stress, and the corresponding absolute energy is the highest. When the cycle times are 0, 50, 75, 100, and 200 times, the number of AE signals released by the concrete specimen in the Na_2SO_4 solution group is 23950, 31384, 30418, 37263, and 41861, respectively. The corresponding maximum absolute energy values are $3.10\text{E}9$ aJ, $1.40\text{E}9$ aJ, $1.20\text{E}9$ aJ, $5.80\text{E}8$ aJ, and $3.20\text{E}8$ aJ, respectively. With the increase of freeze-thaw cycles, the number of AE signals generated by the failure of concrete specimens increases, but the corresponding maximum absolute energy value decreases. The concrete specimens in the Na_2SO_4 solution group are subjected to frost heave force, sulfate crystallization pressure, and

expansion force of erosion products, resulting in the development of internal micro-cracks (Jiang et al., 2015). In the process of compression failure, more AE signals are generated by friction dislocation between cracks. Compared with the particle bonding fracture, the AE signal generated by friction dislocation between cracks is weaker, that is, the energy value decreases (Chen et al., 2019). The analysis based on the AE energy spectrum shows that the internal structural damage and failure mechanism of the two groups of concrete specimens correspond to the changes of AE signals.

3.4. Avalanche characteristics

The AE characterization of avalanche characteristics is mainly the probability density distribution of absolute energy, amplitude, duration, and the correlation distribution of amplitude with absolute energy and duration. Previous studies on coal (Jiang et al., 2016; Xu et al., 2019), sandstone (Zhao et al., 2019; Jiang et al., 2019; Salje et al., 2018), teeth (Wang et al., 2021), and other materials (Chen et al., 2019, 2022) have shown that their probability density distributions of absolute energy, amplitude, and duration conform to the power law in a double logarithmic coordinate. The probability density function of absolute energy can be expressed as (Salje and Dahmen, 2014):

$$P(E)dE \sim \frac{E^{-\varepsilon}}{E_{\min}^{1-\varepsilon}} E > E_{\min} \quad (2)$$

Where E is the absolute energy, E_{\min} is the lower limit for standardization, and ε is the power law exponent, also known as the energy distribution exponent. The definition of the amplitude distribution exponent τ and the duration distribution exponent α is similar to that of the energy distribution exponent ε . In the double logarithmic coordinate system with amplitude on the X-axis and absolute energy on the Y-axis, the amplitude and absolute energy data points of all AE signals also exhibit a power law, with the corresponding power law exponent being the correlation distribution exponent x between amplitude and absolute energy. The definition of the duration and amplitude correlation distribution exponent χ is similar. Due to the large number of AE signals, the amplitude interval is divided into equal exponential intervals in logarithmic coordinates, and the mean value of absolute energy, amplitude and duration of the signals within the divided sub intervals

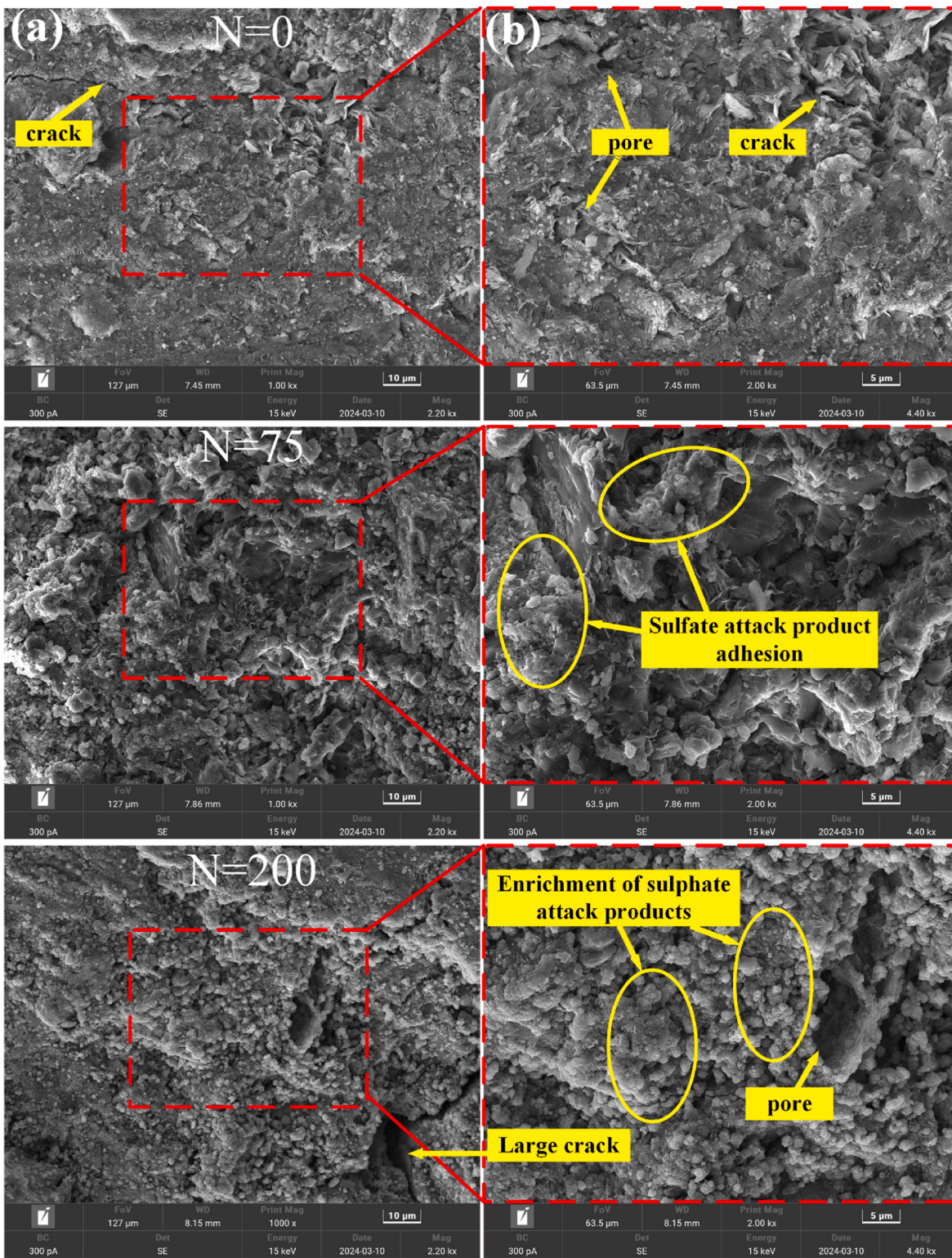


Fig. 5. SEM diagrams of concrete specimens with different cycles under salt-freezing action.

are calculated to make the data graph more concise.

The histogram method is adopted to obtain the probability density distribution of AE absolute energy of concrete specimens under different freeze-thaw cycles, as shown in Fig. 8. The probability density distribution of absolute energy of the two groups of concrete specimens in double logarithm coordinates presents power law distribution, and the corresponding energy distribution exponent increases with the increase of freeze-thaw cycles. Before the test, the energy distribution exponent

of the concrete specimen is 1.48. After 200 cycles, the energy distribution exponent in the Na_2SO_4 solution group and clean water group increased to 1.60 and 1.58, respectively.

The probability density distribution of amplitude and duration of concrete specimens in the Na_2SO_4 solution group and clean water group under different freeze-thaw cycles and the correlation distribution between amplitude and absolute energy and duration are shown in Figs. 9 and 10. In double logarithmic coordinates, the above distributions show

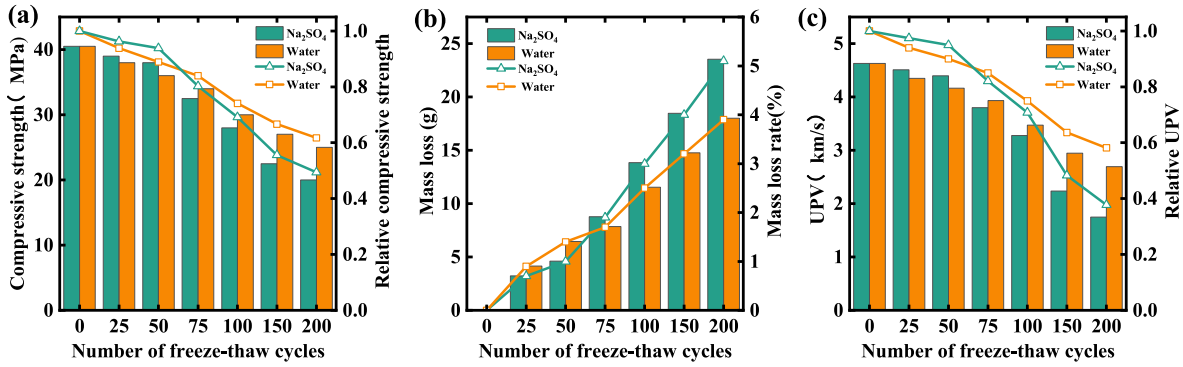


Fig. 6. Physical mechanical properties of concrete specimens under different cycles: (a) compressive strength; (b) mass loss rate; (c) UPV.

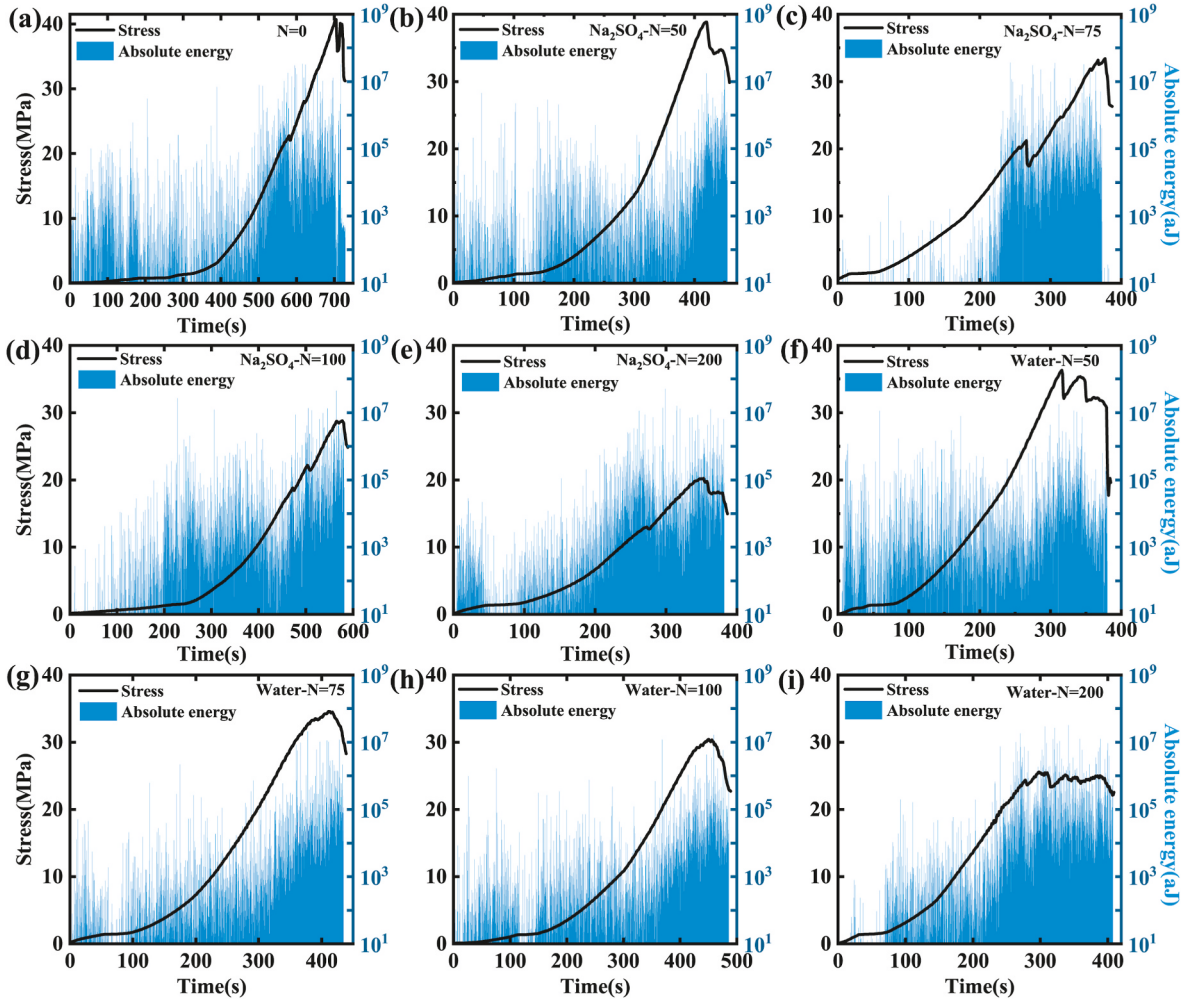


Fig. 7. Stress-time relationship and AE energy spectrum of concrete specimens under different cycles: (a) before the test; (b)–(e) Na₂SO₄ solution group; (f)–(i) clean water group.

power law. In the Na₂SO₄ solution group, when the cycle number is 0, the distribution exponents of the concrete specimen are $\tau = 2.24$, $\alpha = 2.96$, $x = 2.46$, $\chi = 2.54$, respectively. After 200 cycles, the corresponding distribution exponents are $\tau = 2.52$, $\alpha = 3.60$, $x = 2.39$, $\chi = 2.07$, respectively. In the clean water group, after 200 cycles, the distribution exponents are $\tau = 2.47$, $\alpha = 3.36$, $x = 2.36$, $\chi = 2.34$, respectively. With the increase of freeze-thaw cycles, the amplitude distribution exponent and duration distribution exponent of the concrete specimens in the Na₂SO₄ solution group and clean water group

gradually increase, while the correlation exponent between amplitude and absolute energy decreases, and the correlation exponent between duration and amplitude fluctuates within a certain range. The avalanche exponents of concrete in the Na₂SO₄ solution group are slightly larger than that in the clean water group, as shown in Tables 4 and 5. The relationship between the avalanche exponents is more inclined to the force integral average field model $\tau-1 = x(\epsilon-1) = (\alpha-1)/\chi = 1.33$.

According to the definition of probability density distribution, the increase of energy distribution exponent, amplitude distribution

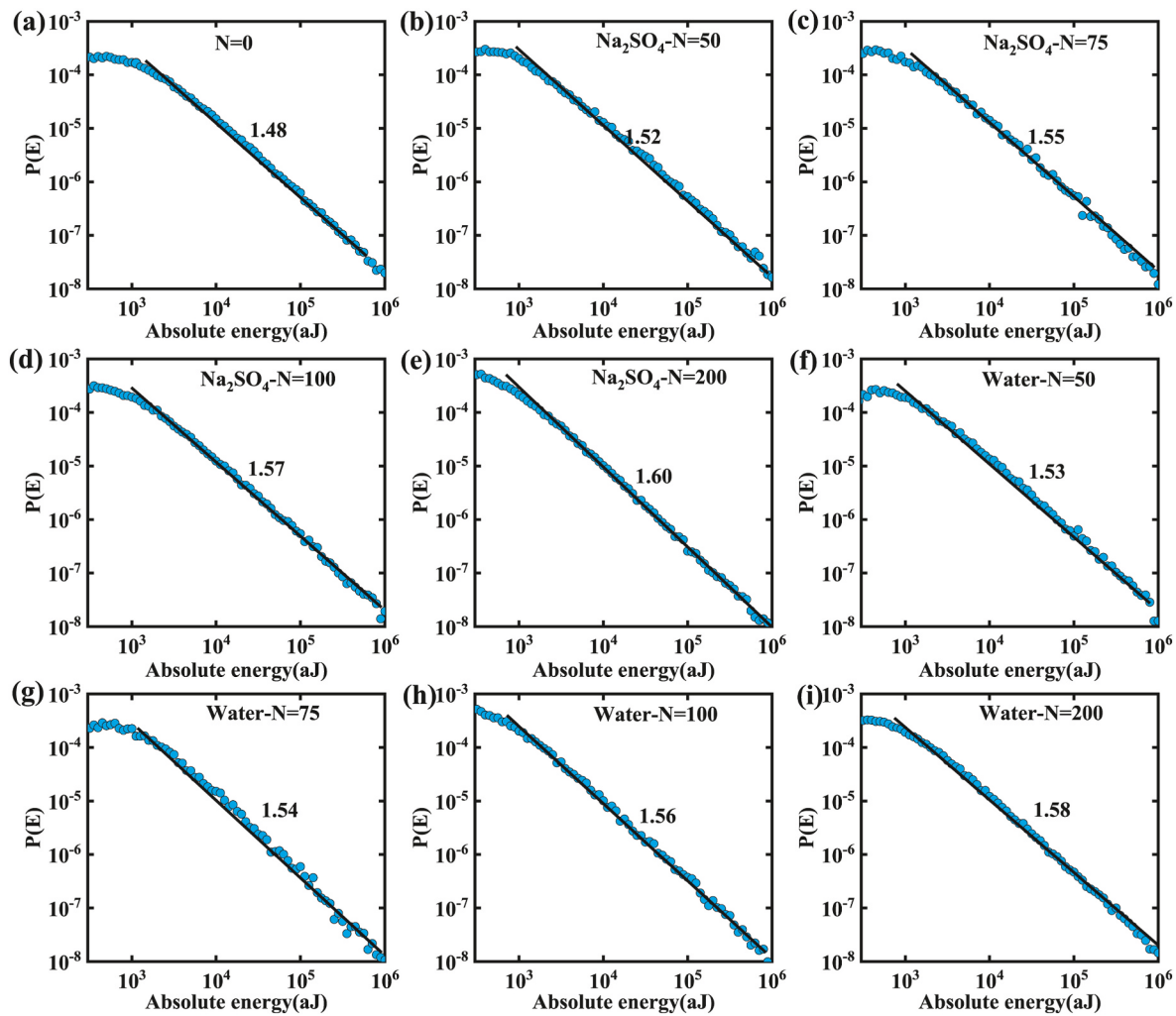


Fig. 8. Probability density distribution of absolute energy of concrete under different cycles: (a) before the test; (b)–(e) Na_2SO_4 solution group; (f)–(i) clean water group.

exponent, and duration distribution exponent indicates that the proportion of weak signals with low energy, small amplitude, and short duration in AE signals increases. Previous study on the avalanche characteristics of Mg-Ho alloys (Chen et al., 2019) have shown that strong signals with high energy, large amplitude, and long duration will be generated by particle bonding fracture and pore collapse, while weak signals will be generated by friction dislocation between particles. With the increase of freeze-thaw cycles, micro-cracks develop inside concrete specimens. During the process of compression failure, friction dislocation between cracks increases, and weak AE signals are generated. The variation of energy distribution exponent of granite under high temperature (Xie et al., 2019) is also similar to that of this experiment. The evolution of the avalanche exponents of concrete specimens reflects the changes of internal mesostructure and failure mechanism.

Fig. 11 shows the probability density distribution of waiting time of concrete specimens in the Na_2SO_4 solution group and clean water group under different freeze-thaw cycles. In this paper, the waiting time δ is defined as the interval between two adjacent AE signals. In the process of statistical analysis, the AE signals are screened by different energy levels ($10^0, 10^1, 10^2, 10^3, 10^4 \text{ aJ}$), and the waiting time is calculated and normalized. $\langle \delta \rangle$ is the average of waiting time. It can be seen from the figure that the probability density distribution of waiting time for different energy levels of each group of concrete specimens is relatively concentrated under different cycle times, showing a double power law distribution. The exponent values of the waiting time distribution in the

medium and large intervals of the Na_2SO_4 solution group are 1.29 and 2.02, respectively, and the corresponding exponent values in the clean water group are 1.36 and 2.29, respectively, which are close to the theoretical values of 1.00 and 2.00. Previous studies on the distribution of waiting time for earthquakes (Jordi et al., 2013) and the waiting time distribution for avalanche events during the failure process of Vycor (SiO_2) (Jordi et al., 2013), coal (Jiang et al., 2016), and sandstone (Zhao et al., 2019) materials have shown that the waiting time distribution for small-scale material damage and large-scale earthquake damage overlap in the same coordinate system, exhibiting a double power law, indicating that the distribution pattern of waiting time has a scale-free distribution characteristic and is a universal law. Furthermore, studies on the avalanche characteristics of granite under thermal damage (Xie et al., 2019) and sandstone under wet-dry cycles (Xie et al., 2018) have shown that the probability density distribution of waiting time is almost unaffected by temperature and the number of wet dry cycles. The distribution of waiting time is less affected by the effect of salt freezing and has a certain robustness, which is similar to the above studies.

3.5. Traditional AE statistical analysis

In seismology, the b -value is used to describe the relationship between earthquake magnitude and frequency, and the corresponding formula is expressed as follows (Choi and Yun, 2015):

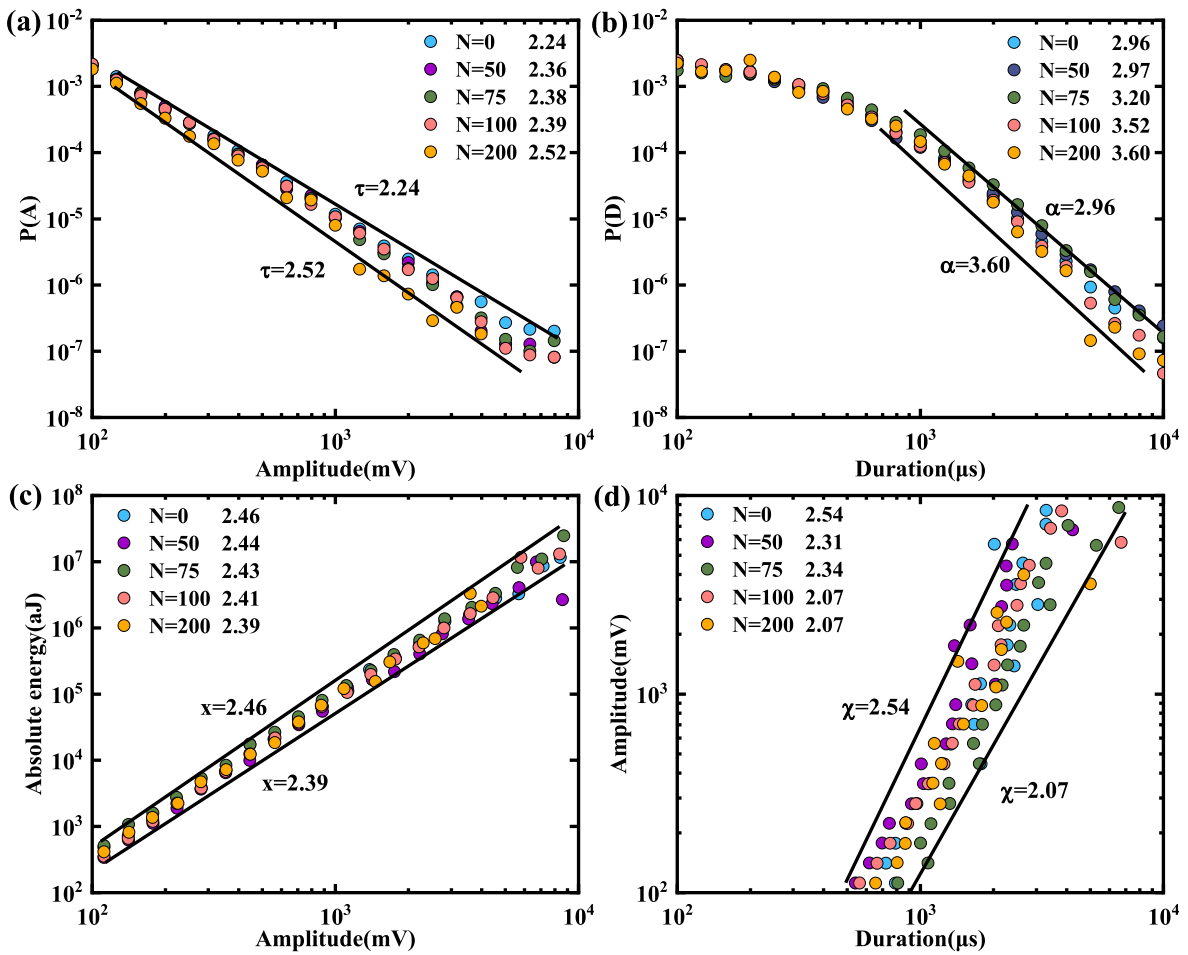


Fig. 9. The probability density distributions of concrete under different cycle times in Na_2SO_4 solution group: (a) amplitude distribution; (b) duration distribution; (c) correlation distribution between amplitude and absolute energy; (d) correlation distribution between amplitude and duration.

$$\log_{10} N = a - bM \quad (3)$$

Where M is the earthquake magnitude, N is the corresponding number of earthquakes, and a is a constant. The mechanism of mesoscale material failure in the laboratory is similar to the earthquake. Statistical analysis of b -value based on AE has been applied to the damage research of rock, concrete, and other materials. The formula for calculating the b -value based on AE is as follows (Xu et al., 2023):

$$\log_{10} N = a - b(A_{db} / 20) \quad (4)$$

Where A_{db} is the maximum amplitude of the AE event. In order to ensure statistical accuracy and make the obtained results more intuitive, the least square method is used to calculate the b -value, and the step is set to 5 dB.

The statistics of the AE overall b -value of concrete specimens in the Na_2SO_4 solution group and clean water group under different freeze-thaw cycles are shown in Fig. 12. The b -value of the two groups of concrete specimens increases with the increase of freeze-thaw cycles, and the increase of the Na_2SO_4 solution group is slightly greater than the clean water group. The b -value of the initial concrete specimen is 1.24. After 200 cycles, the b -value of the Na_2SO_4 solution group and clean water group increases to 1.47 and 1.42 respectively. The proportion of small amplitude AE signal increases, and the corresponding b -value increases. Previous study (Lian et al., 2023) based on nuclear magnetic resonance and AE detection have shown that as the number of freeze-thaw cycles increases, the micro-pores in concrete continue to expand and penetrate into the meso-pores, leading to an increase in the

degree and scale of internal damage and an increase in the b -value, which is similar to this study.

4. Discussion

The size of the b -value is related to the stress state and crack failure scale of the AE source, which can reflect the formation and development of material cracks. Choi et al. (Choi and Yun, 2015) established the relationships between the physical damage levels and the b -value. When the b -value is greater than 1.25, it represents the development of micro-cracks. When the b -value is between 1.15 and 1.25, it represents the propagation of micro-crack and crack widening. When the b -value is between 0.8 and 1.15, it represents the formation of macro-crack and failure. Xu et al. (2023) also pointed out that the b -value reflects the fracture process of concrete well. The initial stage involves the formation and aggregation of micro-cracks, with no macroscopic cracks present. There are more AE events with smaller amplitudes and higher b -values. In the subsequent stage, macroscopic cracks form and propagate, the proportion of large amplitude AE events increases, and the b -value decreases. Finally, in the stage of unstable fracture expansion, the proportion of AE events with larger amplitudes is still relatively high, and the b -value gradually decreases. Statistical analysis of avalanche characteristics of material failure shows that the avalanche exponents are closely related to the internal microstructure and failure mechanism of materials. Xie et al. [49] investigated the internal structure and avalanche characteristics of sandstone under wet-dry cycles using nuclear magnetic resonance and AE detection. The results show that a few micro-pores and micro-cracks inside the sandstone continue to develop

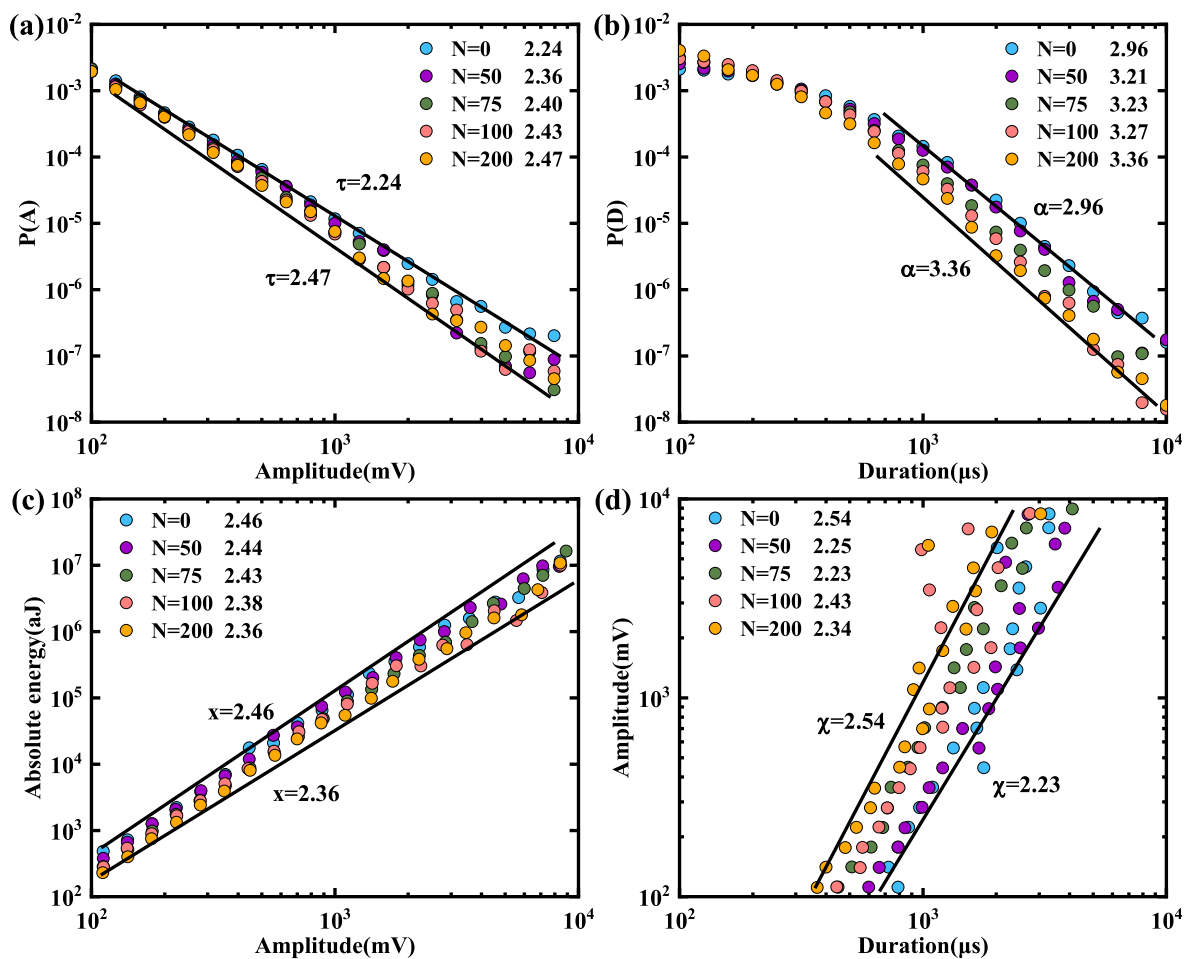


Fig. 10. The probability density distributions of concrete under different cycle times in clean water group: (a) amplitude distribution; (b) duration distribution; (c) correlation distribution between amplitude and absolute energy; (d) correlation distribution between amplitude and duration.

Table 4
Avalanche exponents of representative specimens in Na_2SO_4 solution group.

Avalanche exponent	Theoretical value		Experiment				
	MFM	FI-MFM	0	50	75	100	200
ϵ	1.33	1.67	1.48 ± 0.05	1.52 ± 0.09	1.55 ± 0.07	1.57 ± 0.10	1.60 ± 0.07
τ	1.67	2.33	2.24 ± 0.06	2.36 ± 0.04	2.38 ± 0.07	2.39 ± 0.08	2.52 ± 0.07
α	2	3	2.96 ± 0.05	2.97 ± 0.04	3.20 ± 0.04	3.52 ± 0.07	3.60 ± 0.14
x	2	2	2.46 ± 0.06	2.44 ± 0.04	2.43 ± 0.03	2.41 ± 0.05	2.39 ± 0.03
χ	1.5	1.5	2.54 ± 0.12	2.31 ± 0.19	2.34 ± 0.13	2.07 ± 0.20	2.07 ± 0.18

Note: MFM = mean field model. FI-MFM = force integrated mean field model. The theoretical values are derived from the combination of the micromechanical model of solid deformation and the mean field theory, and refer to References (Zhang et al., 2024) and (Dahmen et al., 2009) for details.

Table 5
Avalanche exponents of representative specimens in clean water group.

Avalanche exponent	Theoretical value		Experiment				
	MFM	FI-MFM	0	50	75	100	200
ϵ	1.33	1.67	1.48 ± 0.05	1.53 ± 0.07	1.54 ± 0.02	1.56 ± 0.09	1.58 ± 0.10
τ	1.67	2.33	2.24 ± 0.06	2.36 ± 0.10	2.40 ± 0.07	2.43 ± 0.04	2.47 ± 0.02
α	2	3	2.96 ± 0.05	3.21 ± 0.10	3.23 ± 0.08	3.27 ± 0.06	3.36 ± 0.11
x	2	2	2.46 ± 0.06	2.44 ± 0.04	2.43 ± 0.02	2.38 ± 0.10	2.36 ± 0.02
χ	1.5	1.5	2.54 ± 0.12	2.25 ± 0.01	2.23 ± 0.13	2.43 ± 0.03	2.34 ± 0.17

and merge after undergoing wet-dry cycles, resulting in an increase in porosity. There is a logarithmic relationship between porosity and avalanche exponent. Similar results have also been reflected in the study of avalanche characteristics of granite under thermal damage (Xie et al.,

2019).

In this paper, the pre-peak stages of compressive failure of the specimen are divided into 10 stages based on the peak stress σ_p . AE signals in each stage are taken as data sets, b -values and amplitude

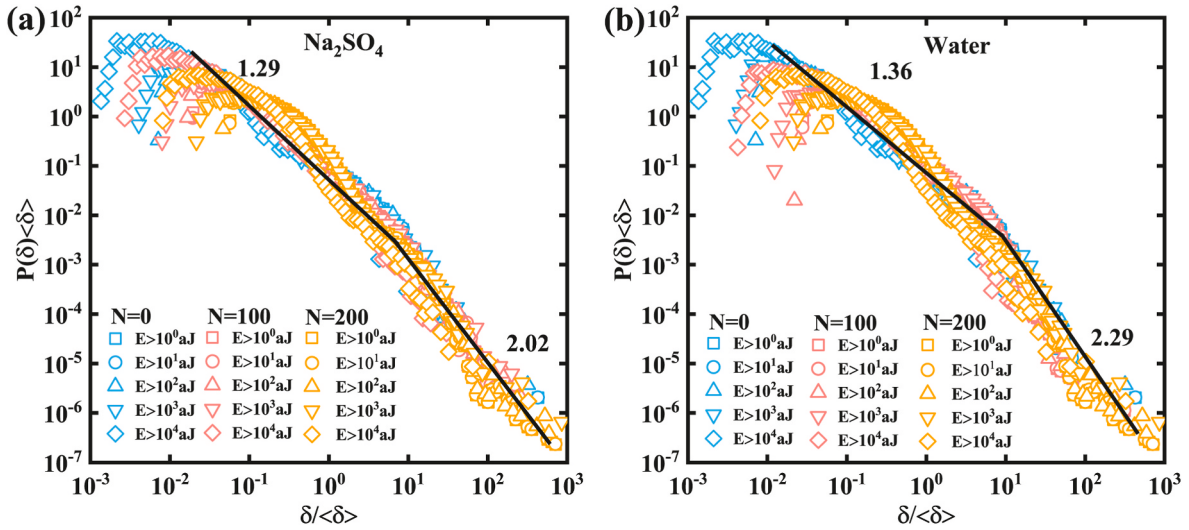


Fig. 11. Probability density distribution of waiting time under different cycles: (a) Na_2SO_4 solution group; (b) clean water group.

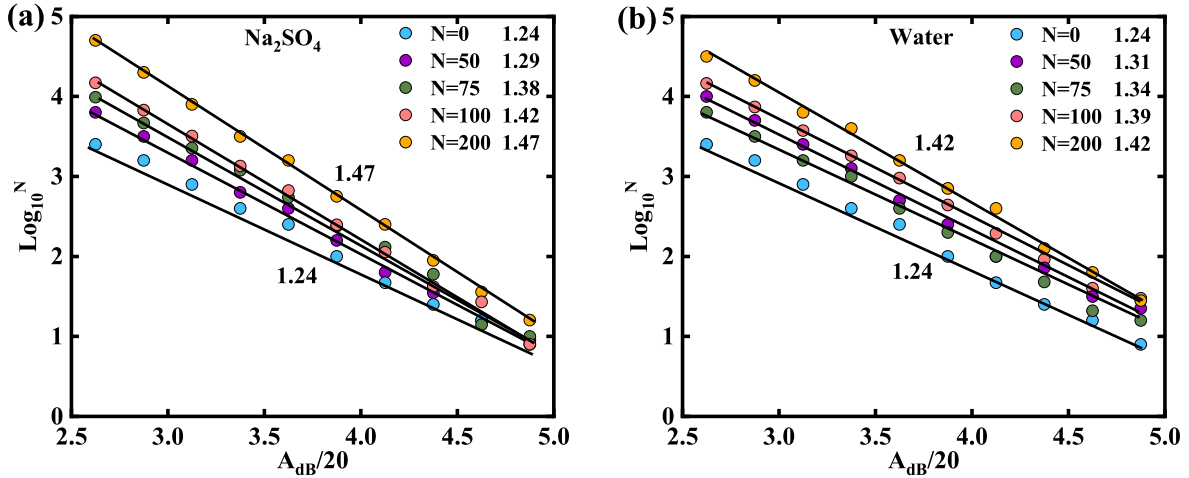


Fig. 12. Distribution of overall b -value under different cycles: (a) Na_2SO_4 solution group; (b) clean water group.

distribution exponent values of each stage are statistically analyzed by least square method, and the relationship curves of b -values and amplitude distribution exponent values of concrete specimens in Na_2SO_4 solution group and clean water group with stress are obtained under different freeze-thaw cycles, as shown in Fig. 13. In the initial state ($N = 0$), the concrete specimen is mainly pore compaction in the initial stage of compression ($0-0.1\sigma_p$ stage), which generates a low amplitude signal and a large b -value. With the increase of stress, micro-cracks in the specimen are generated and gradually connected to form large-scale cracks. The signals of low and high amplitude coexist. The b -value fluctuates within a certain range after decreasing, and the specimen enters a stable damage development stage. When the stress exceeds $0.8\sigma_p$, the micro-cracks in the specimen accumulate and penetrate, the large-scale cracks increase, the proportion of high amplitude signals increases, and the b -value decreases. After the freeze-thaw cycle, the pore compaction stage of the concrete specimens in the Na_2SO_4 solution group is prolonged, and the b -value increases or maintains at a high value during the $0-0.3\sigma_p$ stage. Subsequently, the fluctuation of the b -value of the specimen is weakened and mainly shows a decreasing trend, indicating that the specimen entered a stage of rapid damage development. In the clean water group, the b -value fluctuation of concrete specimens with 50, 75, and 100 cycles is longer, indicating that the stable damage development stage of the specimens is longer. When the

stress exceeds $0.3\sigma_p$, the b -value of the concrete specimen with 200 cycles decreases rapidly, and the specimen enters the stage of rapid damage development earlier. The freeze-thaw cycle and sulfate erosion shorten the stable damage development stage of concrete specimens, and enter the rapid damage development stage earlier.

The variation of amplitude distribution exponent of concrete specimens in the Na_2SO_4 solution group and clear water group is consistent with b -value, indicating that the amplitude distribution exponent can also reflect the formation and development of cracks. However, the b -value evaluation of material damage lacks a uniform threshold, and can not effectively evaluate the damage degree quantitatively. The avalanche exponents based on statistical analysis of avalanche characteristics have theoretical thresholds, and their cross-scale characteristics also provide support for quantitative damage evaluation. Compared with the traditional b -value analysis where amplitude is measured in dB, the avalanche exponents show higher sensitivity in capturing small damage changes, especially in energy distribution exponent statistics where energy is measured in aJ units ($1 \text{ aJ} = 10^{-18} \text{ J}$). Meanwhile, avalanche exponents have diversity, including statistical analysis of parameters such as energy, amplitude, and duration. However, the accurate determination of avalanche exponents requires a large amount of experimental or monitoring data. In addition, this method relies on statistical physical models such as mean field theory, whose assumptions

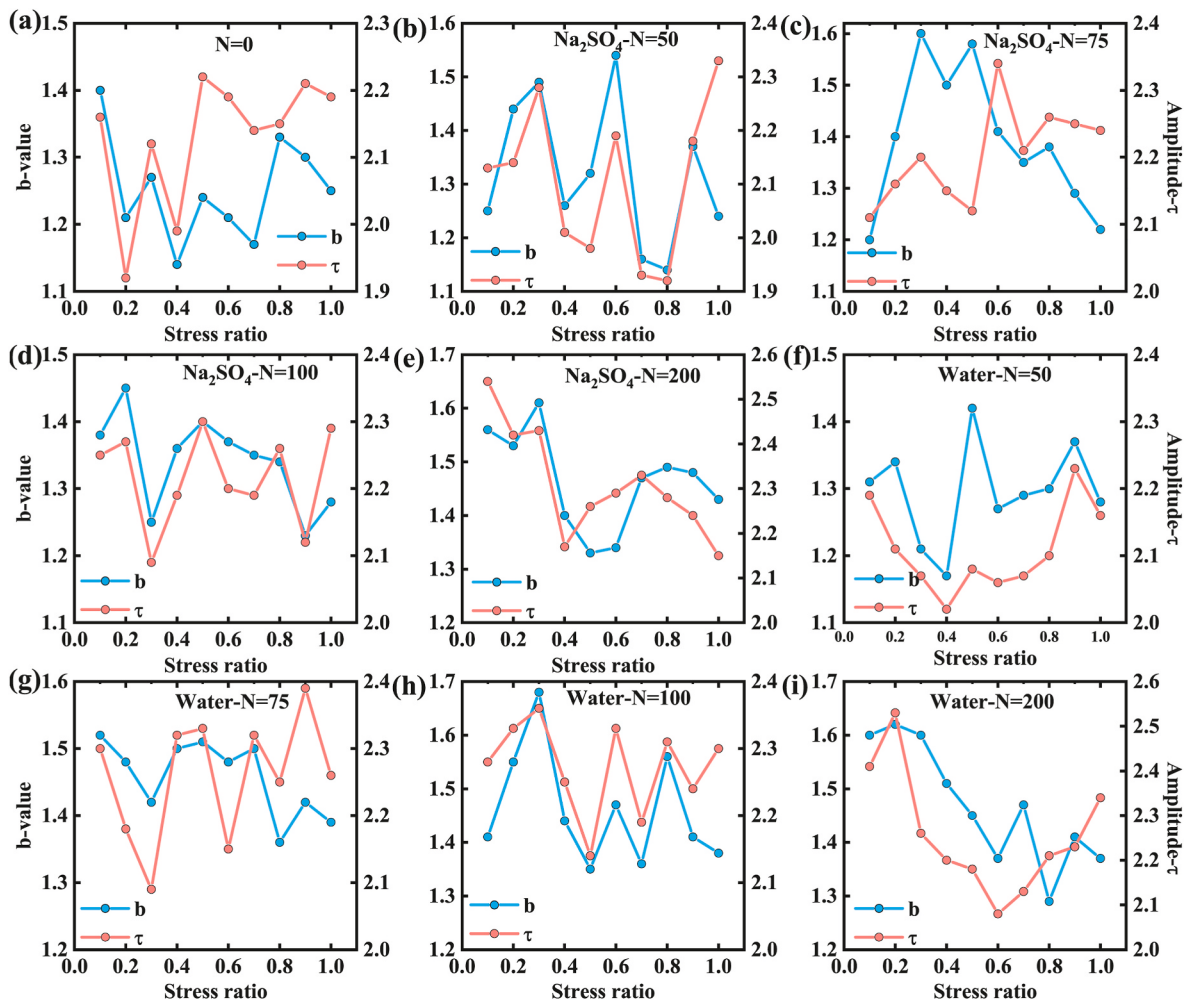


Fig. 13. The variation of b -value and amplitude distribution exponent with stress of concrete specimens under different cycles: (a) before the test; (b)–(e) Na_2SO_4 solution group; (f)–(i) clean water group.

may not be fully applicable to all materials.

5. Conclusion

Based on AE technology and avalanche dynamics theory, the physical mechanical properties and avalanche characteristics of concrete under the coupling action of sulfate attack and freeze-thaw cycles are studied, and compared with traditional AE analysis. The main conclusions are as follows.

- (1) The mass, compressive strength, and UPV of concrete specimens in the Na_2SO_4 solution group and clear water group all decreased with the increase of freeze-thaw cycles. In the initial 50 cycles, the damage degree of the concrete specimens in the clean water group is greater, which indicates that the early sulfate erosion has a certain inhibition effect on the freeze-thaw damage of the specimens. After 75 cycles, the damage degree of concrete specimens in the Na_2SO_4 solution group was larger and increased rapidly, indicating that the damage of concrete by sulfate attack and freeze-thaw cycles promoted each other.
- (2) With the increase of freeze-thaw cycles, the energy distribution exponent, amplitude distribution exponent, and duration distribution exponent of concrete specimens in the Na_2SO_4 solution group and clean water group gradually increased, while the correlation exponent between amplitude and absolute energy decreased, and the correlation exponent between duration and

amplitude fluctuated within a certain range. The avalanche exponents of concrete in the Na_2SO_4 solution group are slightly larger than that in the clean water group. The relationship between the avalanche exponents is more inclined to the force integral average field model. The distribution of waiting time is less affected by the salt-freezing action, which shows a certain robustness.

- (3) The b -value of concrete specimens in the Na_2SO_4 solution group and clear water group increases with the increase of freeze-thaw cycles, and the proportion of shear cracks in the failure process increases gradually. The increase of the Na_2SO_4 solution group is slightly larger than that in the clear water group. The salt-freezing action shorten the stable damage development stage of concrete specimens, and enter the rapid damage development stage earlier. The variation of amplitude distribution exponent of concrete specimens is consistent with b -value, indicating that the amplitude distribution exponent can also reflect the formation and development of cracks. The avalanche exponents have theoretical thresholds and multi-parameter characteristics, which provide support for quantitative damage evaluation.

CRediT authorship contribution statement

Yunfeng Zhao: Writing – review & editing. **Minghui Chen:** Writing – review & editing, Writing – original draft, Investigation, Data curation. **Xiang Jiang:** Investigation. **Xuepeng Cao:** Investigation. **Binbin Qin:**

Investigation.

Declaration of competing interest

The authors declare that they have no known competing financial interests or personal relationships that could have appeared to influence the work reported in this paper.

Acknowledgments

This work was supported by the National Natural Science Foundation of China (No. 52204201, 52178313) and Hubei Province Science and Technology Plan Project (2022BAD151).

Data availability

Data will be made available on request.

References

- Adediran, A., Yliniemi, J., Carvelli, V., et al., 2022. Durability of alkali-activated Fe-rich fayalite slag-based mortars subjected to different environmental conditions[J]. *Cement Concr. Res.* 162, 106984.
- Bai, W., Lu, X., Yuan, C., et al., 2023a. Study on macroscopic mechanical properties and mesoscopic damage mechanism of recycled concrete with metakaolin under sodium sulfate erosion environment. *J. Build. Eng.* 70, 106413.
- Bai, W., Wang, X., Yuan, C., et al., 2023b. Study on dynamic mechanical properties and meso-damage mechanism of carbon fibers recycled aggregate concrete under freeze-thaw environment. *J. Build. Eng.* 79, 107768.
- Bao, W., Yin, Y., Mi, W., et al., 2024. Durability and microstructural evolution of high-performance ecological geopolymer concrete under low-pressure-salt-erosion-freeze-thaw cycling conditions. *Construct. Build. Mater.* 426, 136197.
- Bian, Y., Song, F., Liu, H., et al., 2024. Study on the performance of basalt fiber geopolymer concrete by freeze-thaw cycle coupled with sulfate erosion[J]. *AIP Adv.* 14 (1), 015136.
- Bizzozeri, J., Gosselin, C., Scrivener, K.L., 2014. Expansion mechanisms in calcium aluminate and sulfoaluminate systems with calcium sulfate[J]. *Cement Concr. Res.* 56, 190–202.
- Chen, Y., Ding, X., Fang, D., et al., 2019. Acoustic emission from porous collapse and moving dislocations in granular Mg-Ho alloys under compression and tension[J]. *Sci. Rep.* 9, 1330.
- Chen, D., Deng, Y., Shen, J., et al., 2021. Study on damage rules on concrete under corrosion of freeze-thaw and saline solution. *Construct. Build. Mater.* 304, 124617.
- Chen, Y., Tang, K., Gou, B., et al., 2022. Acoustic emission spectra and statistics of dislocation movements in Fe40Mn40Co10Cr10 high entropy alloys. *J. Appl. Phys.* 132 (8), 080901.
- Choi, W.C., Yun, H.D., 2015. Acoustic emission activity of CFRP-strengthened reinforced concrete beams after freeze-thaw cycling. *Cold Reg. Sci. Technol.* 110, 47–58.
- Dahmen, K.A., Ben-Zion, Y., Uhl, J.T., 2009. Micromechanical model for deformation in solids with universal predictions for stress-strain curves and slip avalanches. *Phys. Rev.* 102, 175501.
- Gan, L., Xu, W., Shen, Z., et al., 2023. Experimental and numerical investigations on damage evolution of concrete under sulfate attack and freeze-thaw cycles. *J. Build. Eng.* 71, 106469.
- Gong, L., Yu, X., Liang, Y., et al., 2023. Multi-scale deterioration and microstructure of polypropylene fiber concrete by salt freezing. *Case Stud. Constr. Mater.* 18, e01762.
- He, J., Qiao, C., Farnam, Y., 2023. Durability evaluation of reinforced concrete with surface treatment of soy methyl ester-polystyrene under freeze-thaw cycles and calcium chloride. *Cement Concr. Compos.* 137, 104927.
- Home Global Symposium on Salt-affected Soils | Food and Agriculture Organization of the United Nations [EB/OI]. <https://www.fao.org/events/global-symposium-on-salt-affected-soils/en>.
- Hu, S., Yin, Y., 2022. Fracture properties of concrete under freeze-thaw cycles and sulfate attack. *Construct. Build. Mater.* 350, 128856.
- Jiang, L., Niu, D., Yuan, L., et al., 2015. Durability of concrete under sulfate attack exposed to freeze-thaw cycles. *Cold Reg. Sci. Technol.* 112, 112–117.
- Jiang, X., Jiang, D., Chen, J., et al., 2016. Collapsing minerals: crackling noise of sandstone and coal, and the predictability of mining accidents[J]. *Am. Mineral.* 101 (12), 2751–2758.
- Jiang, D., Xie, K., Chen, J., et al., 2019. Experimental analysis of sandstone under uniaxial cyclic loading through acoustic emission statistics. *Pure Appl. Geophys.* 176 (1), 265–277.
- Jordi, B., Álvaro, C., Xavier, I., et al., 2013. Statistical similarity between the compression of a porous material and earthquakes. *Phys. Rev. Lett.* 110 (8), 88702.
- Li, Y., Guo, H., Zhou, H., et al., 2022. Damage characteristics and constitutive model of concrete under uniaxial compression after Freeze-Thaw damage. *Construct. Build. Mater.* 345, 128171.
- Lian, S., Zheng, Kun, Zhao, Y., et al., 2023. Investigation the effect of freezethaw cycle on fracture mode classification in concrete based on acoustic emission parameter analysis[J]. *Construct. Build. Mater.* 362, 129789.
- Liu, M., Lu, J., Lou, B., 2023. Research on Kaiser effect of acoustic emission in concrete subjected to bending after freeze-thaw[J]. *J. Build. Eng.* 78, 107713.
- Liu, D., Zhang, W., Jian, Y., et al., 2024. Damage precursors of sulfate erosion concrete based on acoustic emission multifractal characteristics and b-value[J]. *Construct. Build. Mater.* 419, 135380.
- Luo, Q., Liu, D.X., Qiao, P., et al., 2018. Microstructural damage characterization of concrete under freeze-thaw action. *Int. J. Damage Mech.* 27 (10), 1551–1568.
- Müllauer, W., Beddoe, R.E., Heinz, D., 2013. Sulfate attack expansion mechanisms. *Cement Concr. Res.* 52, 208–215.
- Qaidi, S., Dinkha, Y., Haido, J., et al., 2021. Engineering properties of sustainable green concrete incorporating eco-friendly aggregate of crumb rubber: a review. *J. Clean. Prod.* 324, 129251.
- Qaidi, S., Tayeh, B., Zeyad, A., et al., 2022. Recycling of mine tailings for the geopolymers production: a systematic review. *Case Stud. Constr. Mater.* 16, e00933.
- Qiao, Y., Sun, W., Jiang, J., 2015. Damage process of concrete subjected to coupling fatigue load and freeze/thaw cycles. *Construct. Build. Mater.* 93, 806–811.
- Salje, E.K.H., Dahmen, K.A., 2014. Crackling noise in disordered materials[J]. *Annu. Rev. Condens. Matter Phys.* 5 (1), 233–254.
- Salje, E.K.H., Liu, H., Jin, L., et al., 2018. Intermittent flow under constant forcing: acoustic emission from creep avalanches[J]. *Appl. Phys. Lett.* 112 (5), 054101.
- Sethna, J.P., Dahmen, K.A., Myers, C.R., 2001. Crackling noise. *Nature* 410 (6825), 242–250.
- Sun, M., Xin, D., Zou, C., 2019. Damage evolution and plasticity development of concrete materials subjected to freeze-thaw during the load process. *Mech. Mater.* 139, 103192.
- Wang, D., Zhou, X., Meng, Y., et al., 2017. Durability of concrete containing fly ash and silica fume against combined freezing-thawing and sulfate attack. *Construct. Build. Mater.* 147, 398–406.
- Wang, L., Cao, S., Jiang, X., et al., 2021. Cracking of human teeth: an avalanche and acoustic emission study. *J. Mech. Behav. Biomed. Mater.* 122, 104666.
- Wei, Y., Chen, X., Chai, J., et al., 2024. Correlation between mechanical properties and pore structure deterioration of recycled concrete under sulfate freeze-thaw cycles: an experimental study. *Construct. Build. Mater.* 412, 134794.
- Xiao, Q.H., Li, Q., Cao, Z.Y., et al., 2019. The deterioration law of recycled concrete under the combined effects of freeze-thaw and sulfate attack[J]. *Construct. Build. Mater.* 200, 344–355.
- Xie, K., Jiang, D., Sun, Z., et al., 2018. NMR, MRI and AE statistical study of damage due to a low number of wetting-drying cycles in sandstone from the three gorges reservoir area. *Rock Mech. Rock Eng.* 51, 3625–3634.
- Xie, K., Jiang, X., Jiang, D., et al., 2019. Change of crackling noise in granite by thermal damage: monitoring nuclear waste deposits. *Am. Mineral.* 104 (11), 1578–1584.
- Xu, Y., Borrego, A.G., Planes, A., et al., 2019. Criticality in failure under compression: acoustic emission study of coal and charcoal with different microstructures. *Phys. Rev.* 99 (3), 033001.
- Xu, H., Bu, J., Chen, X., et al., 2023. Fracture behavior of dredged sand concrete under freeze-thaw cycles. *Construct. Build. Mater.* 366, 130192.
- Xue, W., Peng, X., Alam, M.S., et al., 2024. Pore structure, mechanical property and permeability of concrete under sulfate attack exposed to freeze-thaw cycles. *Arch. Civ. Mech. Eng.* 24 (2), 130.
- Zhang, H., Ji, S.S., Liu, H., et al., 2024. Research on dynamic splitting tensile damage characteristics of steel fiber reinforced concrete under freeze-thaw cycle environment based on AE. *J. Build. Eng.* 84, 108490.
- Zhao, Y., Liu, H., Xie, K., et al., 2019. Avalanches in compressed sandstone: crackling noise under confinement[J]. *Crystals* 9 (11), 582.
- Zhao, N., Wang, S., Wang, C., et al., 2020. Study on the durability of engineered cementitious composites (ECCs) containing high-volume fly ash and bentonite against the combined attack of sulfate and freezing-thawing (F-T)[J]. *Construct. Build. Mater.* 233, 117313.
- Zhao, N., Wang, S., Quan, X., et al., 2021a. Behavior of polyvinyl alcohol fiber reinforced geopolymer composites under the coupled attack of sulfate and freeze-thaw in a marine environment. *Ocean Engineering* 238, 109734.
- Zhao, Y., Ren, S., Wang, L., et al., 2021b. Acoustic emission and physicomechanical properties of concrete under sulfate attack. *J. Mater. Civ. Eng.* 33 (4), 04021016.
- Zhao, Y., Wang, L., Zeng, L., et al., 2022. Avalanches in concrete compression failure under sulfate attack. *Mater. Struct.* 55 (10), 249.
- Zheng, C., Li, L., Zong, Z., 2024. Study on the sulfate freeze-thaw resistance of recycled coarse aggregate self-compacting concrete[J]. *Structures* 61, 105973.